Feeding Behavior Modifies Daily Rhythms in Autonomic Signaling and Core Body Temperature to Shape 24-hour Rhythms in Cardiac Electrophysiology

Makoto Ono[1], Don E. Burgess[1], Sidney R. Johnson[1], Claude S. Elayi[2], Karyn A. Esser[3], Tanya S. Seward[1], Carie R. Boychuk[4], Andrés P. Carreño[1], Rebecca A. Stalcup[1], Abhilash Prabhat[1], Elizabeth A. Schroder[1,5*], Brian P. Delisle[1*]

[1]Department of Physiology, University of Kentucky, Lexington, KY, USA
[2]CHI Saint Joseph Hospital, Lexington, KY, USA
[3]University of Florida, Gainesville, FL, USA
[4]Dalton Cardiovascular Research Center, Department of Biomedical Sciences, University of Missouri, Columbia, MO, USA
[5]Department of Internal Medicine, University of Kentucky, Lexington, KY, USA

*Contributed equally to the study

Running Title: Shaping 24-hour Rhythms in RR and QT Intervals

Corresponding authors:

Elizabeth A. Schroder
Department of Internal Medicine
859-323-5571
eschr0@uky.edu
780 Rose Street, Medical Science Building, Rm: MN-512, Lexington, KY 40536-0298

Brian P. Delisle
(859) 323-2797
brian.delisle@uky.edu
741 S Limestone Street BBSRB B353, Lexington, KY, 40536

Word Count: 7,974

Key Words: Cardiac Electrophysiology**,** Time of Feeding**,** Core Body Temperature**,** Circadian Rhythms**,** Autonomic Nervous System

Abstract

Circadian rhythms in physiology and behavior are intrinsic ≈24-hour cycles regulated by biological clocks (i.e., circadian clocks) that optimize organismal homeostasis in response to predictable environmental changes. Studies suggest that circadian clock signaling in the suprachiasmatic nucleus of the hypothalamus and cardiomyocytes shape day/night rhythms in cardiac electrophysiology (i.e., RR and QT intervals). However, studies also show that the day/night rhythm of the RR and QT intervals depends on the timing of feeding in mice. This study determined the mechanisms for how feeding impacts day/night rhythms in the RR and QT intervals in mice. Telemetry was used to record electrocardiograms, core body temperature, and activity in mice during ad libitum-fed conditions and after inverting normal feeding behavior by restricting the timing of feeding to the light cycle. Light-cycle restricted feeding caused a simultaneous realignment of RR, QT, and PR intervals and body temperature to the new feeding time. Correcting the QT interval for body temperature eliminated the 24-hour rhythm in the QT interval. Estimating the impact of temperature on RR intervals did not account for the daily change in the RR interval during light-cycle restricted feeding. Cross-correlation analysis suggested daily rhythm in RR intervals correlated with heart rate variability measures but not activity. Injecting mice undergoing light cycle-restricted feeding with propranolol and atropine caused a complete loss in the 24-hour rhythm in the RR interval. We conclude that feeding behavior impacts body temperature and autonomic regulation of the heart to generate 24-hour rhythms in RR and QT intervals.

Abbreviations:

ALF - ad libitum fed
ECG - Electrocardiogram
L-RF - Light cycle restricted feeding
HR - Heart rate – (HR)
HRV - heart rate variability
MAP - Mean arterial pressure
pHF - high-frequency power
pLF - low-frequency power
Tb - core body temperature
SD - standard deviation
WT - Wild type
$QT_{37°C}$ - QT corrected to 37°C
ZT - Zeitgeber Time

New and Noteworthy Our findings demonstrate that feeding behavior is a critical timekeeper for aligning daily rhythms in cardiac electrophysiology (i.e., RR and QT intervals) in mice. The data suggest that feeding behavior shapes 24-hour rhythms in the RR interval by altering day/night rhythms in core body temperature and autonomic input to the heart. In contrast to the RR interval, the 24-hour rhythms in the QT interval are largely shaped by day/night rhythms in core body temperature.

Introduction

Organisms have evolved circadian rhythms in physiology to anticipate predictable changes in the daily environment.(1) In mammals, circadian rhythms are generated at the cellular level by the circadian clock mechanism, a transcription-translation feedback loop that cycles with a periodicity of ≈24 hours.(2, 3) The circadian clock mechanism in the suprachiasmatic nucleus (SCN) of the hypothalamus entrains to the light cycle, and light-entrained SCN neurons signal to neighboring SCN neurons and other brain nuclei to align neurohumoral signaling, behavioral rhythms, and peripheral circadian clocks throughout the body.(4, 5) Several studies suggest SCN signaling modifies autonomic input to the heart to generate day/night rhythms in cardiac electrophysiology (i.e., RR and QT intervals).(6, 7) Studies also show that the circadian clock mechanism in cardiomyocytes contributes to day/night rhythms in the RR and QT intervals by altering the expression of genes, proteins, and different cardiac ionic currents.(8-14)

Feeding behavior is an important timekeeping cue for aligning circadian clocks in peripheral tissues, including the heart. Mouse studies reveal that restricting feeding to the inverse time of normal feeding behavior (i.e., light cycle-restricted feeding) realigns the phase of circadian mRNA expression in the heart and day/night rhythms in cardiac electrophysiology to the new feeding behavior.(15, 16) The effect of light-cycle restricted feeding on the realignment of day/night rhythms in cardiac electrophysiology is not secondary to changes in the circadian clocks in the SCN or cardiomyocytes. The reason is the circadian clock in the SCN remains entrained to the light cycle during light cycle-restricted feeding,(17) and genetic disruption of the cardiomyocyte circadian clock by inducing deletion of BMAL1 does not prevent realignment of day/night rhythms in cardiac electrophysiology with feeding.(18) This study determined the mechanism by which day/night rhythms in cardiac electrophysiology align with feeding behavior.

Previous studies show that light cycle-restricted feeding in mice reduces the day/night rhythm in core body temperature.(17, 19) Several studies show a strong temperature dependence in the RR and QT interval.(20-30) This raises the intriguing possibility that the alignment of day/night rhythms in cardiac electrophysiology to feeding behavior is facilitated by core body temperature.

Methods

Animals. All the mice used in this study were male SV129 mice. Wild type (WT) and *Scn5a*$^{+/\Delta KPQ}$ mice used in longitudinal L-RF studies were 3-4 months old, and mice used for pharmacological studies were 6-8 months old. All procedures complied with the Association for Assessment and Accreditation of Laboratory Animal Care guidelines and were approved by the Institutional Animal Care and Use Committee at the University of Kentucky. Dr. Peter Carmeliet kindly provided the *Scn5a*$^{+/\Delta KPQ}$ mouse strain.(31) This study represents new and reanalyses of data collected previously.(15) All studies were performed at room temperature (23 ± 2°C) except for data presented in **Figure 7**. These mice were housed in thermoneutral temperatures (30 ± 2°C).(32)

Light Cycle Restricted Feeding. Mice were housed in 12-hour light/dark cycles at room temperature with ad libitum access to water. To initiate light cycle restricted feeding (L-RF), food was removed at 9 h after the beginning of the light cycle (Zeitgeber time or ZT

= 9). The next day, food presentation was restricted for 7 h during the light cycle, between ZT 2–9 for up to two weeks unless otherwise noted. L-RF caused mice to lose body mass during the first week (**Figure S1**). However, caloric intake increased after that, and L-RF animals gained body mass after two weeks, similar to previous reports.(33) Telemetry recordings were performed in ad libitum fed conditions (ALF) before L-RF, shortly after starting L-RF, and two weeks after the start of L-RF.

ECG, Tb, and Locomotor Activity Measurements by Telemetry. We used telemetry to measure electrocardiogram (ECG), core body temperature (Tb), and locomotor activity. Mice were anesthetized with isoflurane and implanted with PhysioTel ETA-F10 (Data Sciences International) telemetry transmitter units. ECG telemetry data were recorded at 1000 Hz, and RR and QT interval analyses were done using MATLAB (MathWorks), similar to those previously described.(8, 15, 18) ECG traces recorded for each hour were aligned to the peak of the R wave to generate an ensemble ECG trace. The beginning of the P wave was defined as the point where the slope of the P wave profile changed by more than 0.001 mV/ms; the Q wave was defined as the point where the slope of the profile changed from negative to positive at the base of the QRS complex; the end of the T wave was defined as the point of intersection of T wave maximum slope with baseline.(34)

The hourly mean data for RR, QT, and PR intervals and Tb were fit with the cosine curve function:

$$\text{Interval} = A*\cos[2\pi*t/T - \emptyset] + m$$

to calculate the period (T), the time between the peak amplitudes; acrophase (∅), the phase of the peak amplitude in relation to the start of the light cycle (ZT = 0); the amplitude (A), one-half of the peak to trough amplitude; and the mesor (m), the rhythm adjusted mean.(8, 15, 18)

Heart rate variability (HRV) was calculated as outlined previously.(35) Following Fenske et al. (35), interpolated RR interval time series were generated for spectral analysis and the determination of frequency domain components of HRV. The frequency range used to classify low-frequency component was 0.4-1.5 Hz, and the frequency range to classify high-frequency component was 1.5-4.0 Hz.(35) Power Spectral Density $\mathcal{P}(f)$ has units of power per frequency (ms^2/Hz). The high- and low-frequency components represent the power within a frequency band and are related to the integration:

$$P_{band} = \int_{f_1}^{f_2} \mathcal{P}(f)df$$

The units of the differential cancel the units of frequency, so the units for the high- and low-frequency components are in ms^2. The normalization is based on the discrete version of Parseval's theorem and allows us to consistently approximate the integration for high- and low- frequency components of the variance for the underlying RR time series.(36)

We used cross-correlation between time series to compare the rhythmicity and phase alignment of the RR interval and Tb, the strength of the high frequency (pHF) HRV component, or activity.(37) The RR interval time series lagged against the time series for the Tb, pHF component, or activity. If the time series are in phase, the peak cross-correlation will occur at lag 0. A regular rise and fall in the cross-correlation between variables with a lag of 0 indicates correlated rhythmicity. We used the R function "ccf" to calculate the cross-correlation.(38) The formula used in "ccf" to calculate the cross-correlation between two time series $X(t), Y(t)$ has the form

$$c_{xy}(t) = \frac{1}{n} \sum_{s=\max(1,-t)}^{\min(n-t,n)} [X(s+t) - \bar{X}]\,[Y(s+t) - \bar{Y}]\,,\ r_{xy}(t) = \frac{c_{xy}(t)}{c_{xy}(0)}$$

This study also corrected the hourly mean in the QT interval for Tb. We used an approach similar to that described previously to generate the Tb correction formula.(30) The hourly mean QT intervals were plotted against the corresponding Tb for all data collected in ALF, after the start of L-RF, and two weeks after the start of L-RF. The data were described using linear regression, and the R^2 for a linear relationship was significant for each data set. The average slope of the linear QT-Tb relation was used to derive the correction formula. We corrected the QT intervals to 37°C ($QT_{37°C}$ interval) because 37°C was the daily mean in the Tb for mice in ALF.

$$QT_{37°C} = \text{QT interval} - (4.3 * (37°C - Tb))$$

We demonstrated that the $QT_{37°C}$ interval generated a horizontal line in the corrected $QT_{37°C}$ -Tb plots to validate the formula.

Additionally, we estimated how much the RR interval changes as a function of Tb (RR_{Tb} interval) using a Q_{10} value of 0.40. This value was chosen based on a report that measured the QT_{10} in isolated WT mouse hearts.(24) For the RR_{Tb} interval calculation, we used a reference Tb of 37°C and an RR interval of 116 ms because these were the daily means for WT mice during ALF.

$$RR_{Tb} \text{ interval} = 116 \text{ ms} * (0.40)^{((Tb-37.0)/10)}$$

Propranolol and atropine injections. We assessed the effect of L-RF on RR interval following intraperitoneal (IP) injection of propranolol hydrochloride and atropine sulfate (propranolol and atropine; 10 mg/kg each) to block β-adrenergic and muscarinic receptors, respectively, similar to that previously reported.(39-41) We did longitudinal studies and injected telemetered mice undergoing L-RF at ZT 23.5 (when the daily rhythm in the RR interval peaked) and 9.5 (when the RR interval was at its nadir) for two consecutive days. The L-RF protocol for these mice was to provide food access between ZT 3 and ZT 9. Feeding onset was delayed one hour to separate the food anticipatory decrease in RR interval before feeding from the start of the light cycle.

Statistical analysis. For some graphs, data are shown as the mean and standard deviation of the mean (SD). For other graphs, a data point for each animal is shown with a horizontal bar at the mean. The statistical JTK_CYCLE package was used to confirm statistically significant cyclical rhythms before analyzing the data using cosine waveform curve fitting.(42) Data were analyzed in PRISM (GraphPad). Data between two groups

were analyzed using a T-test, and data sets with more than two groups were analyzed using a 1-way or 2-way ANOVA. Post-hoc testing was done using Šidák. $p<0.05$ was considered significant.

Results

L-RF simultaneously modifies 24-hour rhythms in cardiac electrophysiology and Tb.

This study determined how L-RF in mice impacts daily rhythms in cardiac electrophysiology. We used *in vivo* telemetry to longitudinally record ECG data from mice in ALF, after the onset of L-RF, and after two weeks of L-RF (**Figure 1A**). Data recorded shortly after starting L-RF revealed the acute impact L-RF had on cardiac electrophysiology, and data recorded two weeks after starting L-RF indicated steady-state (i.e., chronic) changes L-RF had on cardiac electrophysiology.(17) The top panel in **Figure 1B** shows a three-day time series for changes in the hourly mean RR interval, the duration of ventricular repolarization (QT interval), and the duration of atrial to ventricular conduction (PR interval). All three of the time series for the hourly mean of the RR, QT, and PR intervals displayed daily rhythms that aligned and peaked at a similar time during the light cycle. However, one day after starting L-RF, the daily rhythms in ECG data exhibited large simultaneous shifts in phase and increases in amplitude. These changes were not transitory and persisted throughout L-RF (i.e., two weeks after the start of L-RF).

Previous studies show that L-RF causes analogous changes in daily Tb rhythms.(17, 43) Therefore, we determined whether L-RF similarly impacted daily rhythms in ECG data and Tb. We directly compared the hourly mean in Tb for the same days as ECG data from mice in ALF, after starting L-RF, and two weeks after starting L-RF (**Figure 1B**). The daily Tb rhythm mirrored daily rhythms in RR, QT, and PR intervals before and after starting L-RF.

The individual ECG and Tb time series recorded from mice in ALF, one day after starting L-RF, and two weeks after starting L-RF were all significant cyclical rhythms that could be well described using cosine curve fitting to calculate acrophase, period mesor, and amplitude (**Figures 1B, 2A, 2B**). Data showed that the acrophase of daily rhythms in RR intervals, QT intervals, PR intervals, and Tb shifted 7-9 hours shortly after starting L-RF. Only small additional changes were seen after two weeks in L-RF. Although L-RF caused abrupt changes in the phase of the ECG and Tb data, the periodicity of daily ECG and Tb rhythms remained ≈24 hours (**Figure 2A**). Compared to data recorded in ALF, the mesor and amplitudes of 24-hour rhythms in RR and QT intervals increased one day after starting L-RF and persisted two weeks after starting L-RF. Analogous changes were seen in the mesor and amplitude of the Tb rhythm. In contrast, L-RF-induced changes in the 24-hour rhythm of the PR interval did not occur immediately, and alterations in mesor and amplitude of the PR interval were only detected two weeks after starting L-RF.

The 24-hour rhythm in the QT interval depends on Tb

Time series data shows that longitudinal changes in the mean QT interval occur parallel to the RR interval and mirror changes in Tb (**Figure 1**). Unlike larger mammals, studies show that the duration of the QT interval in mice is mainly independent of the

249 RR interval.(9, 44-46) Therefore, we quantified the relation between the QT interval and
250 Tb. We identified a strong negative linear relationship between the mean QT interval
251 and Tb recorded from mice in ALF, initially after starting L-RF, and two weeks after
252 starting L-RF (**Figure 3A**).(30) We then used the average slope of linear regression
253 analyses to normalize the QT interval data to 37°C (the average Tb measured in mice in
254 ALF). Normalizing the time series of the QT interval for a Tb of 37°C caused a complete
255 loss in the 24-hour rhythm in the QT interval for mice in ALF and L-RF (**Figure 3B**).

256 To determine the physiological significance of the QT interval dependence on Tb, we
257 studied a transgenic mouse model of long QT type 3 syndrome (*Scn5a*$^{+/\Delta KPQ}$) before
258 and after L-RF **Figure 2S**. We measured ECG properties and Tb in ALF, immediately
259 after starting L-RF, and two weeks after starting L-RF. The changes in the daily rhythms
260 of the ECG and Tb data after starting L-RF were qualitatively and quantitatively similar
261 to those recorded in WT mice (**Figures 1 and 2S**). Cosine fitting analysis of ECG data
262 from the *Scn5a*$^{+/\Delta KPQ}$ mice showed that one day after starting L-RF, there was an
263 immediate shift in the phase for RR intervals, QT intervals, PR intervals, and Tb; an
264 increase in the amplitudes of the rhythms; an increase in the mesor of the RR, QT, and
265 PR intervals; and a decrease in the mesor for Tb (**Figure 3S**). There were some
266 genotype-specific differences in the mesor and amplitude for RR intervals, QT intervals,
267 and Tb between the WT and *Scn5a*$^{+/\Delta KPQ}$ mice (**Figure 3S**). We then calculated the
268 $QT_{37°C}$ interval for *Scn5a*$^{+/\Delta KPQ}$ mice in ALF, after starting L-RF, and two weeks after
269 starting L-RF, and we compared the $QT_{37°C}$ interval data from the *Scn5a*$^{+/\Delta KPQ}$ mice with
270 WT mice (**Figure 3C**). The $QT_{37°C}$ interval was not different between WT and
271 *Scn5a*$^{+/\Delta KPQ}$ mice in ALF (**Figure 3D**). However, after starting L-RF, the $QT_{37°C}$ interval
272 measured in *Scn5a*$^{+/\Delta KPQ}$ mice became longer than the $QT_{37°C}$ interval measured in WT
273 mice. We also identified a genotype-specific difference in how L-RF impacted the $QT_{37°C}$
274 interval in WT and *Scn5a*$^{+/\Delta KPQ}$ mice. In WT mice, L-RF increased the $QT_{37°C}$ interval
275 only after two weeks, but in *Scn5a*$^{+/\Delta KPQ}$ mice, the $QT_{37°C}$ interval increased after one
276 day (**Figure 3D**).

277 *The daily rhythm in the RR interval depends on Tb and autonomic regulation*

278 We next estimated how much of the day/night in the RR interval may be driven by
279 changes in Tb (RR_{Tb} interval). To estimate the RR_{Tb} interval, we used a Q_{10} value for
280 mouse HR (2.5) and the mesor of the RR interval and Tb measured from mice in ALF
281 (116 ms and 37.0°C, respectively). We compared the estimated RR_{Tb} interval with the
282 RR interval measured from WT mice in ALF, immediately after starting L-RF, and two
283 weeks after starting L-RF (**Figure 4A**). The data suggest that the RR_{Tb} interval
284 represented a significant portion of the daily rhythm in the RR interval during ALF and L-
285 RF. However, large difference between the RR_{Tb} and RR interval emerged during the
286 dark cycle during L-RF (**Figure 4**).

287 The 24-hour rhythm in the RR interval is classically thought to reflect changes in
288 efferent signaling from the autonomic nervous system and activity cycles.(6, 47, 48) We
289 quantified changes in autonomic input to the heart by measuring HRV in the frequency
290 domain.(35) We focused on the pHF component as an index for parasympathetic input
291 since L-RF caused an overall slowing of HR. For mice in ALF, the amplitude of the pHF
292 component was higher during the light cycle compared to the dark cycle. One day after

293 starting L-RF, the pHF component increased during the dark cycle (**Figure 4**), and the
294 increase in the pHF component persisted two weeks after starting L-RF.

295 We also measured the time series in activity from mice in ALF, after starting L-RF,
296 and two weeks after starting L-RF (**Figure 4**). In ALF mice, activity is highest during the
297 dark cycle. However, the reduction in activity during the light cycle was less apparent
298 after starting L-RF. The reason was activity profiles showed multiple peaks during the
299 light and dark cycles.

300 The individual mouse three-day time series data for the pHF component and activity
301 rhythms did not show robust significant cyclical rhythms, and were not well described by
302 cosine waveform curve fitting. Therefore, we analyzed the relative rhythmicity between
303 the RR interval and pHF or activity using cross-correlation analyses.(37) As part of the
304 analysis, we included the cross-correlation between RR-Tb. **Figure 5** shows the cross-
305 correlation results for the RR-Tb, RR-pHF, and RR-activity from mice in ALF, one day
306 after starting L-RF, and two weeks after starting L-RF. The RR-Tb and RR-pHF showed
307 correlated rhythmicity that peaked with a lag of 0. A qualitatively similar correlated
308 rhythmicity was seen in the cross-correlation for RR-activity during ALF, but the
309 correlated rhythmicity was lost after starting L-RF. Taken together with the time course
310 of estimated RR_{Tb} intervals, these data suggest that Tb and autonomic signaling shape
311 the daily rhythm in the RR interval for mice in L-RF.

312 To directly test the involvement of increased autonomic signaling as a factor in the
313 dissociation of RR and RR_{Tb} intervals during L-RF, we determined how propranolol and
314 atropine injections impacted the 24-hour rhythm in mean RR interval and Tb from mice
315 in L-RF (fed from ZT 3 to 9). Mice were subjected to L-RF for one week and then
316 injected with propranolol and atropine at ZT 23.5 and 9.5 for two days (**Figure 6A**).
317 Propranolol and atropine injections caused a loss in the daily rhythms of the RR interval
318 and Tb (**Figure 6B**). Propranolol and atropine injections also caused a loss in the
319 difference between the RR_{Tb} interval and RR interval (**Figure 6C**).

320 The L-RF data suggest that the 24-hour rhythm in the RR interval depends on Tb
321 and autonomic regulation, whereas the 24-hour rhythm in the QT interval primarily
322 depends on Tb. Housing mice in thermoneutrality under ALF conditions increases
323 parasympathetic input to the heart to slow HR without causing large changes in Tb.(49)
324 We determined how housing mice in thermoneutrality impacted the daily rhythms in the
325 RR, RR_{Tb}, QT, and $QT_{37°C}$ intervals. Housing mice at thermoneutrality slowed the RR
326 interval and minimially impacted the RR_{Tb} interval to generate a large difference
327 between the RR_{Tb} interval and RR intervals (compare **Figure 4, top left panel** to
328 **Figure 7A**). In contrast to the RR intervals, the QT and $QT_{37°C}$ intervals measured in
329 thermoneutrality were qualitatively similar to the QT and $QT_{37°C}$ intervals measured at
330 room temperature (compare **Figure 3B**, **left panel** to **Figure 7A**). Thermoneutrality had
331 little impact on the linear relationship between the QT interval and Tb, and the slope of
332 the QT-RR relation was similar to that in **Figure 3A**.(30) The $QT_{37°C}$ interval in mice
333 housed at thermoneutrality also generated a horizontal line when plotted as a function
334 of Tb.

335 **Discussion**

We found that one day after starting L-RF, 24-hour rhythms in mean RR intervals, QT intervals, PR intervals, and Tb shifted simultaneously by 7-9 hours to a new phase and remained at this new phase for the duration of L-RF (**Figures 1B, 2A, 2B**). Changes in ECG data mirrored changes in Tb (**Figure 1B**). We identified a strong linear relation between the QT interval and Tb, and normalizing the QT interval for Tb allowed us to identify prolongations in the QT interval independent of Tb in WT and *Scn5a*$^{+/\Delta KPQ}$ mice (**Figure 3**). The increase of the RR interval during L-RF correlated with changes in the estimated RR_{Tb} interval and the pHF component of HRV analysis (but not activity) (**Figures 4, 5**). Repeated inhibition of *β*-adrenergic and muscarinic receptors in mice undergoing L-RF prevented the increase in RR interval and decrease in Tb during the dark cycle- resulting in a loss of 24-hour rhythms in RR intervals and Tb (**Figure 6**). Measuring the RR, RR_{Tb}, QT, and $QT_{37°C}$ intervals in mice housed in thermoneutrality confirmed that autonomic signaling and Tb shaped the daily rhythm in the RR interval. In contrast, the daily rhythm in the QT interval depended primarily on Tb (**Figure 7**).

The 24-hour rhythm in the QT depends on Tb

The QT interval is used clinically to assess risk for certain deadly ventricular arrhythmias.(50) In humans, the QT interval changes as a function of the RR interval, and several formulas can correct the QT interval for HR. There are also QT interval correction formulas in mice.(51) The most commonly used correction formula was derived by measuring the average HR and corresponding QT interval across the 24-hour cycle. We now report a robust linear QT-Tb relation in mice, and normalizing the QT interval for Tb caused a loss in the daily rhythm of the QT interval in mice. We found that housing mice in thermoneutrality caused large changes in the daily rhythm of the RR interval without large changes in the QT interval or the QT-Tb relation. These new data raise the possibility that the daily rhythm in the QT interval in mice primarily reflects Tb and not the RR interval. This concept is consistent with recent studies showing that mice have a weak HR adaptation of the QT interval.(44, 45, 52) The idea that the daily rhythm in the QT interval in mice primarily reflects Tb is also supported by a study showing that the 24-hour rhythm of the QT interval in mice is independent of the RR interval.(9) Tb was not reported in the study, but the observed change in the amplitude of the daily rhythm in the QT interval (4-5 ms) is consistent with a Tb amplitude typically seen in mice (1°C).(53)

We extended our L-RF studies to quantify changes in the QT interval in a transgenic knock-in mouse model that expresses a mutation linked to long QT syndrome in people.(31) Correcting the QT interval for Tb allowed direct comparisons of QT intervals at different Tb across the 24-hour cycle, identified genotype-specific differences in the QT interval independent of Tb, and showed that L-RF caused a prolongation of the QT interval in *Scn5a*$^{+/\Delta KPQ}$ mice (but not WT mice) after only one day of L-RF. The interpretation of these data is different if the QT interval is not normalized for Tb. These studies underscore the importance of monitoring and considering the influence of Tb when measuring QT intervals in mice.

An important question is whether these data may be relevant to humans. Based on previously published data, we propose that the daily rhythm in Tb also contributes to the 24-hour rhythm in the QTc interval observed in people. Several studies report a

380 temperature dependence of the QTc interval in people as 10-15 ms for every 1°C
381 change in Tb.(25-30) The peak-to-trough amplitude in the daily Tb rhythm in people is
382 about 1°C, and the peak-to-trough amplitude in the 24-hour rhythm in the QTc interval is
383 10-20 ms.(54, 55) Future studies that measure the QT interval and Tb across the 24-
384 hour cycle in people will help delineate how much of the 24-hour rhythms in the QTc
385 interval reflect temperature-dependent changes in the properties of ventricular
386 repolarization. Consideration of the influence of Tb on the QTc interval is warranted
387 when the Tb might be different due to physiological, behavioral, environmental, or
388 pharmacological changes (for example patients with hypothermia or sepsis).

389 *The 24-hour rhythm in the RR interval is primarily shaped by Tb and autonomic*
390 *signaling*

391 Studies suggested that the circadian clock in the SCN modified autonomic signaling
392 to generate the 24-hour rhythm in HR.(6, 56-59) These studies were supported by data
393 showing that ablation of the SCN or transgenic mice lacking the core circadian clock
394 transcription factor *Bmal1* (e.g., *Bmal1*$^{-/-}$) did not have a 24-hour rhythm in HR.(60-62)
395 L-RF is not thought to impact the circadian clock mechanism in the SCN;(17) therefore,
396 it was surprising that L-RF caused a significant phase shift in the 24-hour rhythm of the
397 HR.(15) L-RF in mice also shifts the phase of circadian gene expression in peripheral
398 tissues, including the heart, to align with the timing of feeding behavior.(17) Several
399 studies implicate the cardiomyocyte circadian clock in regulating gene expression
400 essential for cardiac excitability, cardiac electrophysiology, and HR.(8-12, 61, 63) One
401 might predict that L-RF shifts the phase of cardiomyocyte gene expression to facilitate
402 the changes in 24-hour rhythms of HR. However, genetically disrupting the
403 cardiomyocyte-specific circadian clock (by inducing the deletion of *Bmal1*) does not
404 abolish the L-RF-mediated phase shift in the 24-hour rhythm of HR.(18) These data
405 suggest that the observed changes in HR with L-RF are not secondary to changes in
406 cardiomyocyte circadian clock signaling intrinsic to the heart. The autonomic receptor
407 blockade studies suggest that the changes in the 24-hour rhythms of HR before and
408 after L-RF appear to be secondary to autonomic receptor-mediated signaling and Tb.

409 *Implications*

410 Modern lifestyles disrupt evolutionarily conserved behavioral and environmental
411 timekeeping cues critical for maintaining healthy circadian homeostatic
412 mechanisms.(64) Our findings suggest that feeding behavior is a critical timekeeping
413 cue for daily Tb and cardiac electrophysiology rhythms in mice. If conserved, modern
414 lifestyles that disrupt evolutionary conserved feeding rhythms in people may negatively
415 impact the alignment between daily circadian and cardiac electrophysiological rhythms
416 to impair cardiac performance and influence arrhythmogenic risk.

417 Another implication of this study is that it underscores the importance that daily
418 rhythms in Tb have in shaping 24-hour rhythms in cardiac electrophysiology.
419 Continuous monitoring of Tb is not routinely performed in people undergoing
420 electrophysiological testing despite representing an essential contributor to the HR and
421 QTc intervals. This is especially true in studies that monitor changes in HR and QTc
422 intervals across the 24-hour cycle.

Limitations

These studies were performed in mice at room temperature, and fasting mice housed at room temperature makes them vulnerable to torpor (a transient hibernating-like state that causes a significant drop in Tb below 32°C and HR).(23) Our model of L-RF did not calorically restrict the mice, and the mice continued to eat 3-4 grams of food per day during L-RF (**Figure 1S**) and gained mass after one week (**Figure 1S**). Another limitation is that this study used only male mice. We chose male mice because female mice are more prone to torpor.(23) It remains unclear whether a long $QT_{37°C}$ interval is associated with an increased risk for spontaneous ventricular arrhythmias. The lack of spontaneous arrhythmias in *Scn5a*$^{+/\Delta KPQ}$ mice during the short duration of the study is not surprising because the absolute incidence of spontaneous arrhythmias in these mice is very low, similar to humans with LQT3. We found that, during L-RF, the daily rhythm in the PR interval simultaneously shifted with the RR and QT intervals and Tb. However, due to the small amplitude and relatively slow change in the PR interval in response to L-RF, it was difficult to determine if the PR interval reflected Tb, autonomic regulation of the heart, or both. Lastly, caution must be used when extrapolating data from mice to humans.(46, 65)

Summary

Daily rhythms in HR and cardiac electrophysiology align with feeding and activity cycles via signals originating from the SCN. However, when food availability becomes restricted to the light cycle, this disrupts the association between environmental and behavioral timekeeping cues, and daily rhythms in HR and cardiac electrophysiology align with the new feeding behavior and Tb. We conclude that L-RF-induced changes in daily autonomic signaling and Tb rhythms facilitate the realignment of 24-hour rhythms in HR and QT intervals.

Competing interests

None declared.

Author contributions

All authors contributed to drafting the work and revising it critically for important intellectual content, approved the final version of the manuscript, and qualified for authorship.

Funding

This work was supported by National Heart Lung and Blood Institute grants R01HL153042 and R01HL141343.

Data Availability

Data will be made available upon reasonable request.

Acknowledgment

We would like to thank Drs. Wayne Giles and Chao-Yin Chen (University of California, Davis) for providing feedback and discussion. We would also like to acknowledge Isabel Stumpf (Centre College) and David Schneider (Centre College) for technical assistance.

467 **References**

468 1. **Thosar SS, and Shea SA**. Circadian control of human cardiovascular function.
469 *Curr Opin Pharmacol* 57: 89-97, 2021.
470 2. **Mohawk JA, Green CB, and Takahashi JS**. Central and peripheral circadian
471 clocks in mammals. *Annu Rev Neurosci* 35: 445-462, 2012.
472 3. **Mohawk JA, and Takahashi JS**. Cell autonomy and synchrony of
473 suprachiasmatic nucleus circadian oscillators. *Trends Neurosci* 34: 349-358, 2011.
474 4. **Buijs RM, and Kalsbeek A**. Hypothalamic integration of central and peripheral
475 clocks. *Nat Rev Neurosci* 2: 521-526, 2001.
476 5. **Hastings MH, Maywood ES, and Brancaccio M**. Generation of circadian
477 rhythms in the suprachiasmatic nucleus. *Nat Rev Neurosci* 19: 453-469, 2018.
478 6. **Tong M, Watanabe E, Yamamoto N, Nagahata-Ishiguro M, Maemura K,
479 Takeda N, Nagai R, and Ozaki Y**. Circadian expressions of cardiac ion channel genes
480 in mouse might be associated with the central clock in the SCN but not the peripheral
481 clock in the heart. *Biol Rhythm Res* 44: 519-530, 2013.
482 7. **Scheer FA, Ter Horst GJ, van Der Vliet J, and Buijs RM**. Physiological and
483 anatomic evidence for regulation of the heart by suprachiasmatic nucleus in rats. *Am J
484 Physiol Heart Circ Physiol* 280: H1391-1399, 2001.
485 8. **Schroder EA, Burgess DE, Zhang X, Lefta M, Smith JL, Patwardhan A,
486 Bartos DC, Elayi CS, Esser KA, and Delisle BP**. The cardiomyocyte molecular clock
487 regulates the circadian expression of Kcnh2 and contributes to ventricular
488 repolarization. *Heart Rhythm* 12: 1306-1314, 2015.
489 9. **Gottlieb LA, Larsen K, Halade GV, Young ME, and Thomsen MB**. Prolonged
490 QT intervals in mice with cardiomyocyte-specific deficiency of the molecular clock. *Acta
491 Physiol (Oxf)* 233: e13707, 2021.
492 10. **Delisle BP, Stumpf JL, Wayland JL, Johnson SR, Ono M, Hall D, Burgess
493 DE, and Schroder EA**. Circadian clocks regulate cardiac arrhythmia susceptibility,
494 repolarization, and ion channels. *Curr Opin Pharmacol* 57: 13-20, 2021.
495 11. **D'Souza A, Wang Y, Anderson C, Bucchi A, Baruscotti M, Olieslagers S,
496 Mesirca P, Johnsen AB, Mastitskaya S, Ni H, Zhang Y, Black N, Cox C, Wegner S,
497 Bano-Otalora B, Petit C, Gill E, Logantha S, Dobrzynski H, Ashton N, Hart G,
498 Zhang R, Zhang H, Cartwright EJ, Wisloff U, Mangoni ME, da Costa Martins PA,
499 Piggins HD, DiFrancesco D, and Boyett MR**. A circadian clock in the sinus node
500 mediates day-night rhythms in Hcn4 and heart rate. *Heart Rhythm* 18: 801-810, 2021.
501 12. **Jeyaraj D, Haldar SM, Wan X, McCauley MD, Ripperger JA, Hu K, Lu Y,
502 Eapen BL, Sharma N, Ficker E, Cutler MJ, Gulick J, Sanbe A, Robbins J,
503 Demolombe S, Kondratov RV, Shea SA, Albrecht U, Wehrens XH, Rosenbaum DS,
504 and Jain MK**. Circadian rhythms govern cardiac repolarization and arrhythmogenesis.
505 *Nature* 483: 96-99, 2012.
506 13. **Schroder EA, Wayland JL, Samuels KM, Shah SF, Burgess DE, Seward T,
507 Elayi CS, Esser KA, and Delisle BP**. Cardiomyocyte Deletion of Bmal1 Exacerbates
508 QT- and RR-Interval Prolongation in Scn5a (+/ΔKPQ) Mice. *Front Physiol* 12: 681011,
509 2021.

14. **Schroder EA, Lefta M, Zhang X, Bartos DC, Feng HZ, Zhao Y, Patwardhan A, Jin JP, Esser KA, and Delisle BP**. The cardiomyocyte molecular clock, regulation of Scn5a, and arrhythmia susceptibility. *Am J Physiol Cell Physiol* 304: C954-965, 2013.
15. **Schroder EA, Burgess DE, Manning CL, Zhao Y, Moss AJ, Patwardhan A, Elayi CS, Esser KA, and Delisle BP**. Light phase-restricted feeding slows basal heart rate to exaggerate the type-3 long QT syndrome phenotype in mice. *Am J Physiol Heart Circ Physiol* 307: H1777-1785, 2014.
16. **Zhang D, Colson JC, Jin C, Becker BK, Rhoads MK, Pati P, Neder TH, King MA, Valcin JA, Tao B, Kasztan M, Paul JR, Bailey SM, Pollock JS, Gamble KL, and Pollock DM**. Timing of Food Intake Drives the Circadian Rhythm of Blood Pressure. *Function (Oxf)* 2: zqaa034, 2021.
17. **Damiola F, Le Minh N, Preitner N, Kornmann B, Fleury-Olela F, and Schibler U**. Restricted feeding uncouples circadian oscillators in peripheral tissues from the central pacemaker in the suprachiasmatic nucleus. *Genes Dev* 14: 2950-2961, 2000.
18. **Schroder EA, Burgess DE, Johnson SR, Ono M, Seward T, Elayi CS, Esser KA, and Delisle BP**. Timing of food intake in mice unmasks a role for the cardiomyocyte circadian clock mechanism in limiting QT-interval prolongation. *Chronobiol Int* 1-10, 2021.
19. **Schibler U, Gotic I, Saini C, Gos P, Curie T, Emmenegger Y, Sinturel F, Gosselin P, Gerber A, Fleury-Olela F, Rando G, Demarque M, and Franken P**. Clock-Talk: Interactions between Central and Peripheral Circadian Oscillators in Mammals. *Cold Spring Harb Symp Quant Biol* 80: 223-232, 2015.
20. **Clark AJ**. The effect of alterations of temperature upon the functions of the isolated heart. *J Physiol* 54: 275-286, 1920.
21. **Tanner JM**. The relationships between the frequency of the heart, oral temperature and rectal temperature in man at rest. *J Physiol* 115: 391-409, 1951.
22. **Kirschen GW, Singer DD, Thode HC, Jr., and Singer AJ**. Relationship between body temperature and heart rate in adults and children: A local and national study. *Am J Emerg Med* 38: 929-933, 2020.
23. **Swoap SJ, and Gutilla MJ**. Cardiovascular changes during daily torpor in the laboratory mouse. *Am J Physiol Regul Integr Comp Physiol* 297: R769-774, 2009.
24. **Wu Y, Wang Q, Granger J, Gaido OR, Aguilar EN, Ludwig A, Moroni A, Bianchet MA, and Anderson ME**. HCN channels sense temperature and determine heart rate responses to heat. *bioRxiv* 2023.
25. **Fleming PR, and Muir FH**. Electrocardiographic changes in induced hypothermia in man. *Br Heart J* 19: 59-66, 1957.
26. **Hicks CE, McCord MC, and Blount SG, Jr.** Electrocardiographic changes during hypothermia and circulatory occlusion. *Circulation* 13: 21-28, 1956.
27. **Karjalainen J, and Viitasalo M**. Fever and cardiac rhythm. *Arch Intern Med* 146: 1169-1171, 1986.
28. **Mattu A, Brady WJ, and Perron AD**. Electrocardiographic manifestations of hypothermia. *Am J Emerg Med* 20: 314-326, 2002.
29. **Yaganti VM, Naik CA, and Dhond AJ**. Electrocardiographic manifestations in a hypothermic patient: review of Osborn waves. *Indian Heart J* 59: 80-82, 2007.
30. **van der Linde HJ, Van Deuren B, Teisman A, Towart R, and Gallacher DJ**. The effect of changes in core body temperature on the QT interval in beagle dogs: a

556 previously ignored phenomenon, with a method for correction. *Br J Pharmacol* 154:
557 1474-1481, 2008.
558 31. **Nuyens D, Stengl M, Dugarmaa S, Rossenbacker T, Compernolle V, Rudy Y,**
559 **Smits JF, Flameng W, Clancy CE, Moons L, Vos MA, Dewerchin M, Benndorf K,**
560 **Collen D, Carmeliet E, and Carmeliet P**. Abrupt rate accelerations or premature beats
561 cause life-threatening arrhythmias in mice with long-QT3 syndrome. *Nature Medicine* 7:
562 1021-1027, 2001.
563 32. **Skop V, Guo J, Liu N, Xiao C, Hall KD, Gavrilova O, and Reitman ML**. Mouse
564 Thermoregulation: Introducing the Concept of the Thermoneutral Point. *Cell Rep* 31:
565 107501, 2020.
566 33. **Bray MS, Ratcliffe WF, Grenett MH, Brewer RA, Gamble KL, and Young ME**.
567 Quantitative analysis of light-phase restricted feeding reveals metabolic dyssynchrony in
568 mice. *Int J Obes (Lond)* 37: 843-852, 2013.
569 34. **Lund K, Nygaard H, and Kirstein Pedersen A**. Weighing the QT intervals with
570 the slope or the amplitude of the T wave. *Ann Noninvasive Electrocardiol* 7: 4-9, 2002.
571 35. **Fenske S, Probstle R, Auer F, Hassan S, Marks V, Pauza DH, Biel M, and**
572 **Wahl-Schott C**. Comprehensive multilevel in vivo and in vitro analysis of heart rate
573 fluctuations in mice by ECG telemetry and electrophysiology. *Nat Protoc* 11: 61-86,
574 2016.
575 36. **Press WH, and Numerical Recipes Software (Firm)**. Numerical recipes in C.
576 Cambridge, England ; New York, N.Y.: Cambridge University Press,, 1992, p. 1
577 computer disk 5 1/4 in.
578 37. **Levine JD, Funes P, Dowse HB, and Hall JC**. Signal analysis of behavioral and
579 molecular cycles. *BMC Neurosci* 3: 1, 2002.
580 38. **Team Rc**. R: A Language and Environment for Statistical Computing R
581 Foundation for Statistical Computing. https://www.R-project.org.
582 39. **Rose RA, Kabir MG, and Backx PH**. Altered heart rate and sinoatrial node
583 function in mice lacking the cAMP regulator phosphoinositide 3-kinase-gamma. *Circ*
584 *Res* 101: 1274-1282, 2007.
585 40. **Krishnaswamy PS, Egom EE, Moghtadaei M, Jansen HJ, Azer J, Bogachev**
586 **O, Mackasey M, Robbins C, and Rose RA**. Altered parasympathetic nervous system
587 regulation of the sinoatrial node in Akita diabetic mice. *J Mol Cell Cardiol* 82: 125-135,
588 2015.
589 41. **Egom EE, Vella K, Hua R, Jansen HJ, Moghtadaei M, Polina I, Bogachev O,**
590 **Hurnik R, Mackasey M, Rafferty S, Ray G, and Rose RA**. Impaired sinoatrial node
591 function and increased susceptibility to atrial fibrillation in mice lacking natriuretic
592 peptide receptor C. *J Physiol* 593: 1127-1146, 2015.
593 42. **Hughes ME, Hogenesch JB, and Kornacker K**. JTK_CYCLE: an efficient
594 nonparametric algorithm for detecting rhythmic components in genome-scale data sets.
595 *J Biol Rhythms* 25: 372-380, 2010.
596 43. **Satoh Y, Kawai H, Kudo N, Kawashima Y, and Mitsumoto A**. Time-restricted
597 feeding entrains daily rhythms of energy metabolism in mice. *Am J Physiol Regul Integr*
598 *Comp Physiol* 290: R1276-1283, 2006.
599 44. **Mulla W, Murninkas M, Levi O, and Etzion Y**. Incorrectly corrected? QT interval
600 analysis in rats and mice. *Front Physiol* 13: 1002203, 2022.

601 45. **Mulla W, Gillis R, Murninkas M, Klapper-Goldstein H, Gabay H, Mor M,**
602 **Elyagon S, Liel-Cohen N, Bernus O, and Etzion Y**. Unanesthetized Rodents
603 Demonstrate Insensitivity of QT Interval and Ventricular Refractory Period to Pacing
604 Cycle Length. *Front Physiol* 9: 897, 2018.
605 46. **Ripplinger CM, Glukhov AV, Kay MW, Boukens BJ, Chiamvimonvat N,**
606 **Delisle BP, Fabritz L, Hund TJ, Knollmann BC, Li N, Murray KT, Poelzing S, Quinn**
607 **TA, Remme CA, Rentschler SL, Rose RA, and Posnack NG**. Guidelines for
608 assessment of cardiac electrophysiology and arrhythmias in small animals. *Am J*
609 *Physiol Heart Circ Physiol* 323: H1137-H1166, 2022.
610 47. **Barazi N, Polidovitch N, Debi R, Yakobov S, Lakin R, and Backx PH**.
611 Dissecting the Roles of the Autonomic Nervous System and Physical Activity on
612 Circadian Heart Rate Fluctuations in Mice. *Front Physiol* 12: 692247, 2021.
613 48. **Gordan R, Gwathmey JK, and Xie LH**. Autonomic and endocrine control of
614 cardiovascular function. *World J Cardiol* 7: 204-214, 2015.
615 49. **Swoap SJ, Li C, Wess J, Parsons AD, Williams TD, and Overton JM**. Vagal
616 tone dominates autonomic control of mouse heart rate at thermoneutrality. *Am J Physiol*
617 *Heart Circ Physiol* 294: H1581-1588, 2008.
618 50. **Postema PG, and Wilde AA**. The measurement of the QT interval. *Curr Cardiol*
619 *Rev* 10: 287-294, 2014.
620 51. **Mitchell GF, Jeron A, and Koren G**. Measurement of heart rate and Q-T
621 interval in the conscious mouse. *Am J Physiol* 274: H747-751, 1998.
622 52. **Roussel J, Champeroux P, Roy J, Richard S, Fauconnier J, Le Guennec JY,**
623 **and Thireau J**. The Complex QT/RR Relationship in Mice. *Sci Rep* 6: 25388, 2016.
624 53. **Refinetti R**. Circadian rhythmicity of body temperature and metabolism.
625 *Temperature (Austin)* 7: 321-362, 2020.
626 54. **Molnar J, Zhang F, Weiss J, Ehlert FA, and Rosenthal JE**. Diurnal pattern of
627 QTc interval: how long is prolonged? Possible relation to circadian triggers of
628 cardiovascular events. *J Am Coll Cardiol* 27: 76-83, 1996.
629 55. **Browne KF, Prystowsky E, Heger JJ, Chilson DA, and Zipes DP**.
630 Prolongation of the Q-T interval in man during sleep. *Am J Cardiol* 52: 55-59, 1983.
631 56. **Scheer FA, Hilton MF, Mantzoros CS, and Shea SA**. Adverse metabolic and
632 cardiovascular consequences of circadian misalignment. *Proc Natl Acad Sci U S A* 106:
633 4453-4458, 2009.
634 57. **Sano H, Hayashi H, Makino M, Takezawa H, Hirai M, Saito H, and Ebihara S**.
635 Effects of suprachiasmatic lesions on circadian rhythms of blood pressure, heart rate
636 and locomotor activity in the rat. *Jpn Circ J* 59: 565-573, 1995.
637 58. **Schroder EA, and Delisle BP**. Time Restricted Feeding to the Light Cycle
638 Dissociates Canonical Circadian Clocks and Physiological Rhythms in Heart Rate. *Front*
639 *Pharmacol* 13: 910195, 2022.
640 59. **Warren WS, Champney TH, and Cassone VM**. The suprachiasmatic nucleus
641 controls the circadian rhythm of heart rate via the sympathetic nervous system. *Physiol*
642 *Behav* 55: 1091-1099, 1994.
643 60. **Curtis AM, Cheng Y, Kapoor S, Reilly D, Price TS, and Fitzgerald GA**.
644 Circadian variation of blood pressure and the vascular response to asynchronous
645 stress. *Proc Natl Acad Sci U S A* 104: 3450-3455, 2007.

646 61. **Schroder EA, Ono M, Johnson SR, Rozmus ER, Burgess DE, Esser KA, and**
647 **Delisle BP**. The role of the cardiomyocyte circadian clocks in ion channel regulation
648 and cardiac electrophysiology. *J Physiol* 600: 2037-2048, 2022.
649 62. **Yang G, Chen L, Grant GR, Paschos G, Song WL, Musiek ES, Lee V,**
650 **McLoughlin SC, Grosser T, Cotsarelis G, and FitzGerald GA**. Timing of expression
651 of the core clock gene Bmal1 influences its effects on aging and survival. *Sci Transl*
652 *Med* 8: 324ra316, 2016.
653 63. **Hayter EA, Wehrens SMT, Van Dongen HPA, Stangherlin A, Gaddameedhi**
654 **S, Crooks E, Barron NJ, Venetucci LA, Neill JSO, Brown TM, Skene DJ, Trafford**
655 **AW, and Bechtold DA**. Distinct circadian mechanisms govern cardiac rhythms and
656 susceptibility to arrhythmia. *Nat Commun* 12: 2472, 2021.
657 64. **Gohari A, Wiebe D, and Ayas N**. Shift working and cardiovascular health.
658 *Chronobiol Int* 40: 27-32, 2023.
659 65. **Sabir IN, Killeen MJ, Grace AA, and Huang CL**. Ventricular arrhythmogenesis:
660 insights from murine models. *Prog Biophys Mol Biol* 98: 208-218, 2008.
661
662

663 **Figure Legends**
664
665 **Figure 1. L-RF causes a simultaneous shift in the daily rhythms of the RR, QT,**
666 **and PR intervals, Tb, and strength of the pHF component. A.** Representative hourly
667 ensemble ECG traces recorded from a mouse in ALF (left), after initially starting L-RF
668 (middle), or 2 weeks after starting L-RF (right). **B.** Averaged time series data showing 3
669 consecutive days of the hourly mean for the RR interval (vermillion), QT interval (sky
670 blue), PR interval (orange), and Tb (reddish purple). The data are plotted as a function
671 of ZT and the shaded regions correspond to the dark cycle. Left column shows the data
672 recorded during ALF, middle column shows the data recorded initially after starting L-RF
673 (boxed arrow indicates 24 hours after the start of L-RF), and right column shows the
674 data recorded 2 weeks after starting L-RF. The solid lines shown for the time series
675 ECG and Tb data in ALF, 24 hours after the start of L-RF, and 2 weeks after the start of
676 L-RF are cosine curve fit to the averaged data (n = 6 mice, data points are averaged
677 data and SD).
678
679 **Figure 2. L-RF causes a simultaneous shift and increased amplitude in the 24-**
680 **hour rhythms of the mean RR, QT, and PR intervals and Tb.** The individual mouse
681 time series data for the RR, QT, and PR intervals, and Tb were fit to a cosine wave to
682 calculate the acrophase, period, mesor, and amplitude for mice in ALF, 24 hours after
683 initially starting L-RF ($L\text{-}RF_i$), and 2 weeks after starting L-RF ($L\text{-}RF_{2wk}$). **A.** The top row
684 shows the acrophase of the RR interval (vermillion), QT interval (sky blue), PR interval
685 (orange), and Tb (reddish purple) for each condition. The second row, left graph, shows
686 the difference in the acrophase of the RR interval, QT interval, PR interval, and Tb
687 measured from mice in ALF compared to those from mice 24 hours after initially starting
688 L-RF or 2 weeks after starting L-RF. The second row, right graph, shows the period of
689 the RR interval, QT interval, PR interval, and Tb from mice in ALF, 24 hours after
690 initially starting L-RF, and 2 weeks after starting L-RF. **B.** The top row shows the mesor
691 and the second row shows the amplitude of the RR interval, QT interval, PR interval,
692 and Tb for each condition (n = 6 mice per group, *$p<0.05$, **$p<0.01$, ***$p<0.001$,
693 ****$p<0.0001$. The horizontal bar in each data set is the mean).
694
695 **Figure 3. Correcting the QT-interval for Tb causes a loss in the daily rhythm in the**
696 **QT interval. A.** Left graph shows the hourly mean in the QT interval plotted as a
697 function of the corresponding Tb for each mouse in ALF, initially after starting L-RF, or 2
698 weeks after starting L-RF (each mouse is represented by a different color, n = 6). The
699 right graph shows the $QT_{37°C}$ interval is plotted as a function of the corresponding Tb for
700 the same set of mice. Linear regression of the data for each mouse (red lines) was used
701 to calculate the average slope and R^2 and SD for both the left and right graphs. **B.**
702 Averaged time series for the hourly mean $QT_{37°C}$ interval and SD (sky blue) in ALF,
703 initially after starting L-RF (boxed arrow indicates 24 hours after the start of L-RF), and
704 2 weeks after the start of L-RF. Also shown is the corresponding averaged time series
705 data for the hourly mean in the uncorrected QT interval data from **Figure 1** for direct
706 comparison (grey). Data are plotted as a function of ZT and the shaded regions
707 represent the dark cycle. **C.** Averaged time series for the $QT_{37°C}$ interval measured from
708 WT (grey) *Scn5a*$^{+/\Delta KPQ}$ mice (blue). The left column shows the data recorded during

709 ALF, the middle column shows the data recorded initially after starting L-RF (boxed
710 arrow indicates 24 hours after starting L-RF), and the right column shows the data
711 recorded 2 weeks after starting L-RF. Also shown are the mean $QT_{37°C}$ interval
712 measured from WT (grey) from panel **B.** for direct comparison. **D.** The graph shows the
713 average of the mean $QT_{37°C}$ interval measured from WT (grey) or *Scn5a*$^{+/\Delta KPQ}$ mice
714 (blue) in ALF, one day after starting L-RF, and two weeks after starting L-RF. The
715 horizontal bar in each data set is the mean (n = 6, *p<0.05).
716
717 **Figure 4. Day/night rhythm changes in the RR interval during L-RF are not only**
718 **due to Tb.** The top row of graphs show the averaged time series data for 3 consecutive
719 days of the hourly mean for the RR interval from **Figure 1** (grey) overlayed with the
720 RR_{Tb} interval (green). Left column shows the data recorded during ALF, middle column
721 shows the data recorded initially after starting L-RF (boxed arrow indicates 24 hours
722 after the start of L-RF), and right column shows the data recorded 2 weeks after starting
723 L-RF. The middle row of graphs show the corresponding data for pHF (blue), and the
724 bottom row of graphs show the corresponding data for cage activity (yellow). Data are
725 plotted as a function of ZT and the shaded regions correspond to the dark cycle (n = 6
726 mice, data points are averaged data and SD).
727
728 **Figure 5. Cross-correlation analysis between the RR interval and Tb or strength of**
729 **the pHF component shows correlated and aligned rhythmicity.** The average of the
730 cross-correlation between the time series data for the RR interval and Tb (top row,
731 reddish purple), pHF component (middle row, blue), and activity (bottom row, yellow) in
732 ALF (left column), 24 hours after initially starting L-RF (middle column), and 2 weeks
733 after starting L-RF (right column). The peak correlation coefficient at lag 0 is shown (n =
734 6 mice per group, data points are mean data and SD, *p<0.05 and **p<0.01).
735
736 **Figure 6. Propranolol and atropine prevent the daily rhythms in RR interval and**
737 **Tb in mice during L-RF. A.** Time series data showing the hourly mean in the RR
738 interval (vermillion) and Tb (reddish purple) was recorded 1 week after the start of L-RF
739 (ZT 3 to ZT 9). The data are plotted as a function of ZT and the shaded regions
740 represent the dark cycle. The time series shows the average of the hourly mean data
741 and SD measured during the light and dark cycle the day before starting the propranolol
742 and atropine injections (LC0, DC0), and the first and second light and dark cycles after
743 injecting mice at ZT 23.5 and ZT 9.5 (LC1, DC1, LC2, and DC2, respectively, injection
744 times are denoted by arrows; n = 5 mice). **B.** Shown are the mean RR interval
745 (vermillion) and Tb (reddish purple) data recorded during the light and dark cycle the
746 day before (LC0 and DC0) or the days after starting the injections with propranolol and
747 atropine (LC1, DC1, LC2 and DC2; horizontal bar in each data set is the mean, *p<0.05;
748 ***p<0.001). **C.** Time series of RR interval data from **A.** overlayed with the averaged
749 time series for the corresponding RR_{Tb} interval (blue) before and after injection with
750 propranolol and atropine.
751
752 **Figure 7. Housing mice in thermoneutrality alters the daily rhythm in the RR**
753 **interval with minimal impact on the daily rhythm in the QT interval. A.**
754 Representative hourly ensemble ECG traces recorded from a mouse in thermoneutrality

755 at ZT 4 and 17. Also shown are the averaged time series data for 3 consecutive days of
756 the hourly mean for the RR (sky blue), RR_{Tb} (blue), QT (purple), and $QT_{37°C}$ (vermillion)
757 intervals measured from mice in ALF and housed in thermoneutrality. Data are plotted
758 as a function of ZT and the shaded regions correspond to the dark cycle (n = 6 mice,
759 data points are averaged data and SD). **B.** The top graph shows the hourly mean in the
760 QT interval plotted as a function of the corresponding Tb for each mouse in ALF and
761 house in thermoneutrality (each mouse is represented by a different color, n = 6). The
762 bottom graph shows the $QT_{37°C}$ interval is plotted as a function of the corresponding Tb
763 for the same set of mice in the top graph. Linear regression of the data for each mouse
764 (red lines) was used to calculate the average slope, R^2 and SD for both the left and right
765 graphs.
766
767
768
769

Supplemental Material

Supplemental Figure Legends

Figure 1S. L-RF initially causes a decrease in mass, but the mice regain and increase mass after 1 week in L-RF. The left graph shows the daily body mass of mice in ALF (yellow) or after initially starting L-RF (blueish green, n = 5 mice per group, **p<0.01 ***p<0.001); the middle graph shows the average weekly mass in mice during the first 2 weeks of L-RF (n = 6, *p<0.05 and **p<0.01); and the right graph shows the average food consumption per mouse/day during each day after the start of L-RF for 2 weeks (n=6).

Figure 2S. L-RF impacts the daily rhythms of the RR, QT, and PR intervals and Tb in *Scn5a*$^{+/\Delta KPQ}$ mice. A. Representative of hourly ensemble ECG traces recorded from WT or *Scn5a*$^{+/\Delta KPQ}$ mice in ALF (left), after initially starting L-RF (middle), or 2 weeks after starting L-RF (right) at different ZT. The top row shows the times of day when the QT intervals were the longest (peak of rhythm), and the bottom row corresponds to the times of day when the QT intervals were the shortest (nadir of rhythm). **B.** Averaged time series (n = 6 mice, data points are mean data and SD) data showing 3 consecutive days of the hourly mean for the RR interval (vermillion), QT interval (sky blue), PR interval (orange), Tb (reddish purple). Also shown are the RR, QT, and PR intervals measured from WT (grey) from Figure 1 for direct comparison. The data are plotted as a function of ZT, and the shaded regions correspond to the dark cycle.

Figure 3S. L-RF causes genotype-specific differences in the 24-hour rhythms of the mean RR, QT, and PR intervals and Tb measured from WT and *Scn5a*$^{+/\Delta KPQ}$ mice. The individual mouse time series data for the RR, QT, and PR intervals, and Tb were fit to a cosine wave to calculate the acrophase, mesor, and amplitude for *Scn5a*$^{+/\Delta KPQ}$ mice in ALF, 24 hours after initially starting L-RF (L-RF$_i$), and 2 weeks after starting L-RF (L-RF$_{2wk}$). **A.** Shown are the data for the acrophase, **B.** mesor, and **C.** amplitude of the RR interval (vermillion), QT interval (sky blue), PR interval (orange), and Tb (reddish purple) measured from *Scn5a*$^{+/\Delta KPQ}$ mice for each condition. The horizontal bar in each data set is the mean. Also included are the corresponding WT data presented in Figure 2 (grey) for direct comparison (n = 6 mice per group, *p<0.05, **p<0.01, ***p<0.001, ****p<0.0001).

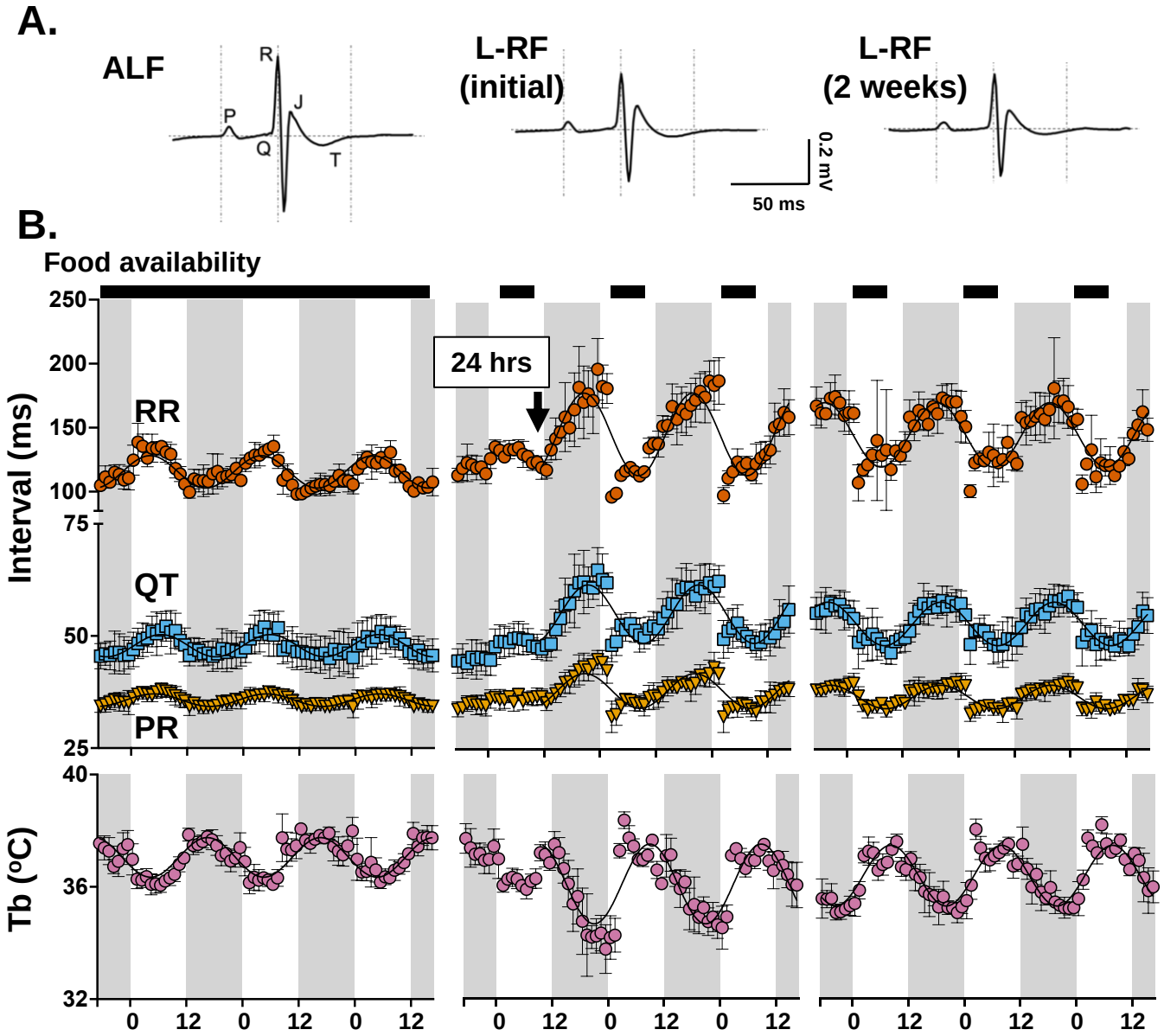
A.
ALF
R
P
J
Q
T
L-RF
(initial)
L-RF
(2 weeks)
0.2 mV
50 ms
B.
Food availability
24 hrs
RR
QT
PR
Interval (ms)
250
200
150
100
75
50
25
Tb (°C)
40
36
32
0
12
0
12
0
12
0
12
0
12
0
12
0
12
0
12
0
12

Figure 1.

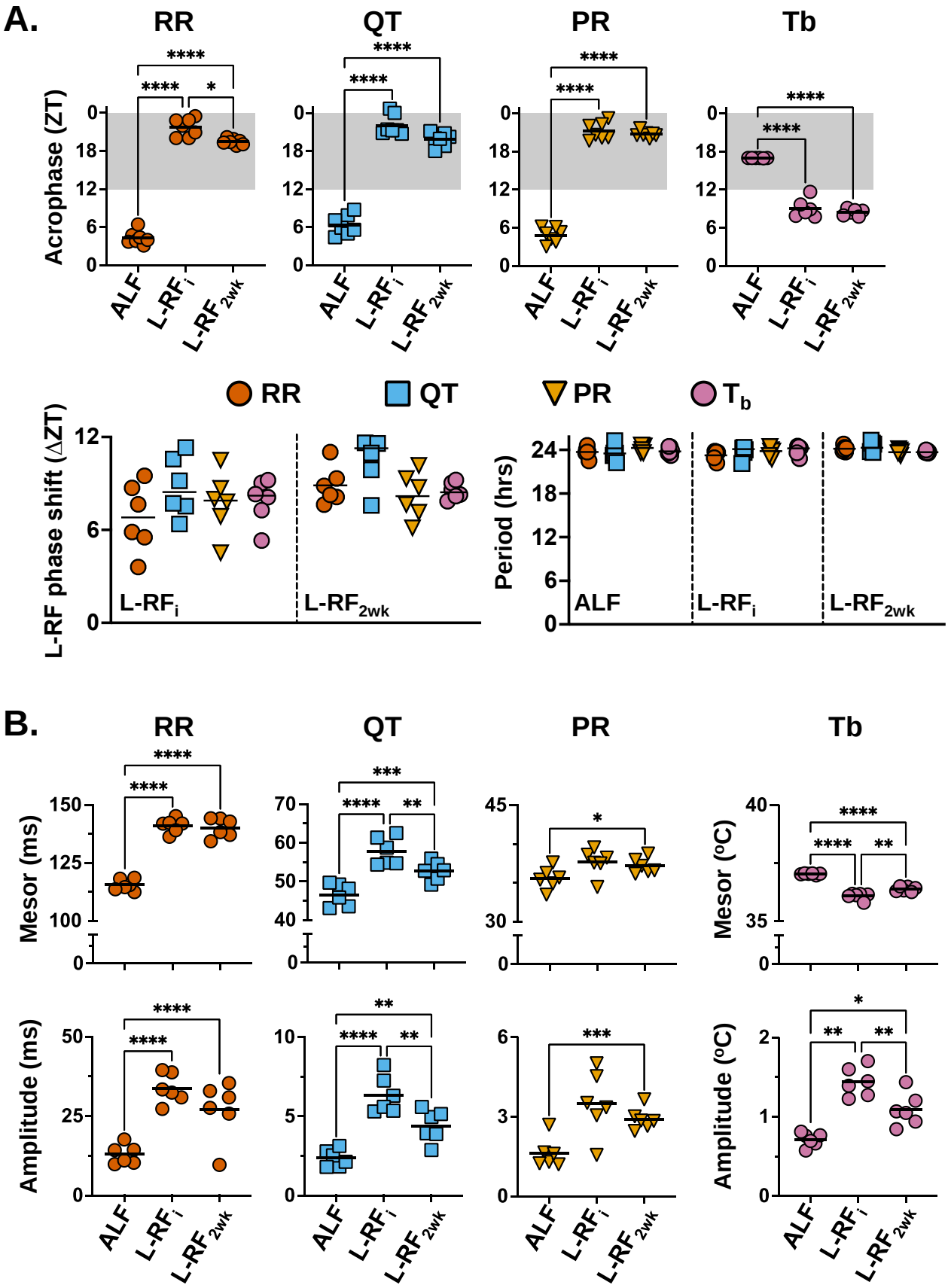
A.
RR
QT
PR
Tb
Acrophase (ZT)
ALF
L-RF$_i$
L-RF$_{2wk}$
RR
QT
PR
T$_b$
L-RF phase shift (ΔZT)
L-RF$_i$
L-RF$_{2wk}$
Period (hrs)
ALF
L-RF$_i$
L-RF$_{2wk}$
B.
RR
QT
PR
Tb
Mesor (ms)
Mesor (°C)
Amplitude (ms)
Amplitude (°C)
ALF
L-RF$_i$
L-RF$_{2wk}$

Figure 2.

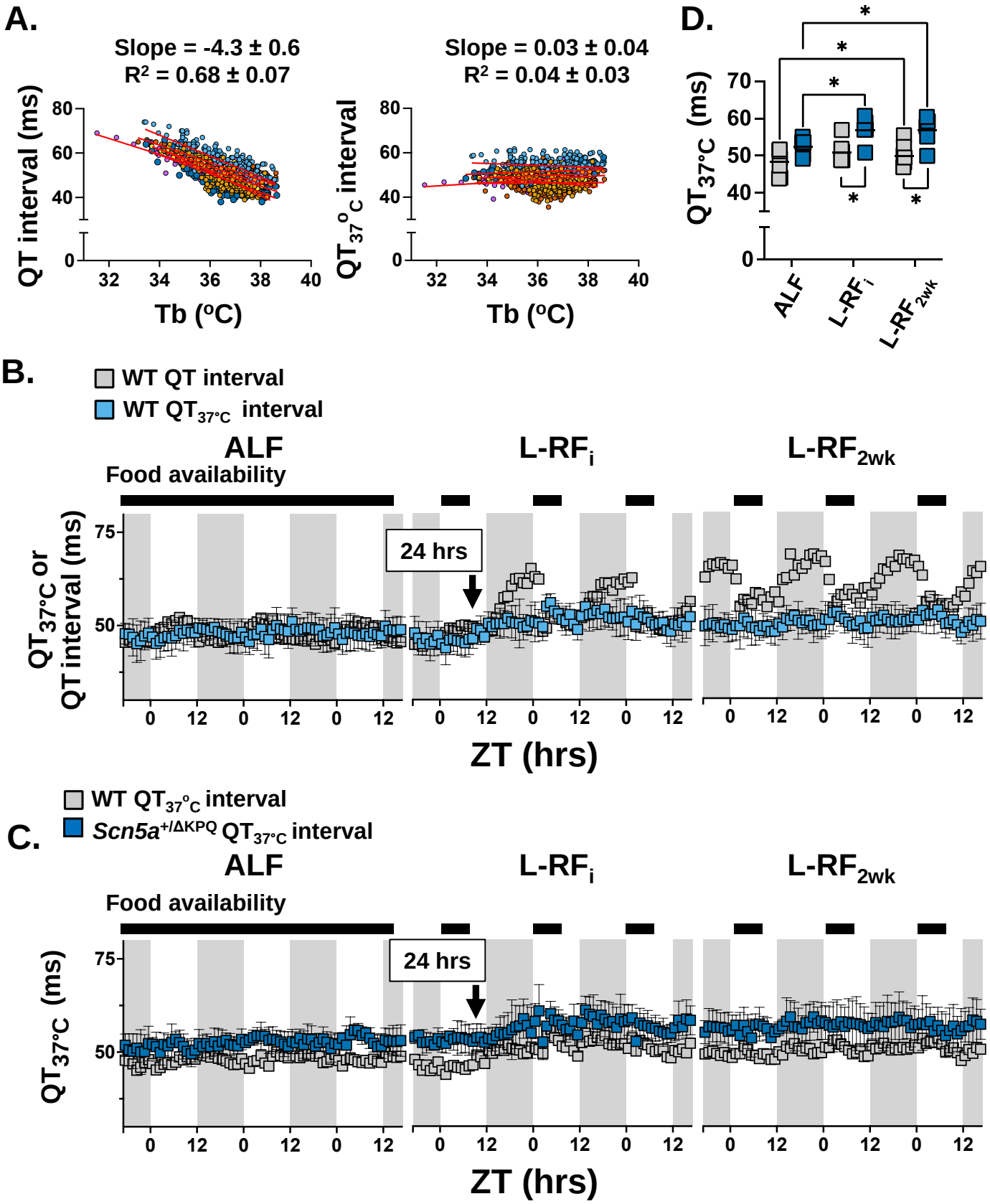
A.
Slope = -4.3 ± 0.6
R² = 0.68 ± 0.07
QT interval (ms)
Tb (ºC)
Slope = 0.03 ± 0.04
R² = 0.04 ± 0.03
QT37ºC interval
Tb (ºC)
D.
QT37ºC (ms)
ALF
L-RFi
L-RF2wk
B.
WT QT interval
WT QT37ºC interval
ALF
L-RFi
L-RF2wk
Food availability
24 hrs
QT37ºC or QT interval (ms)
ZT (hrs)
C.
WT QT37ºC interval
Scn5a+/ΔKPQ QT37ºC interval
ALF
L-RFi
L-RF2wk
Food availability
24 hrs
QT37ºC (ms)
ZT (hrs)

Figure 3.

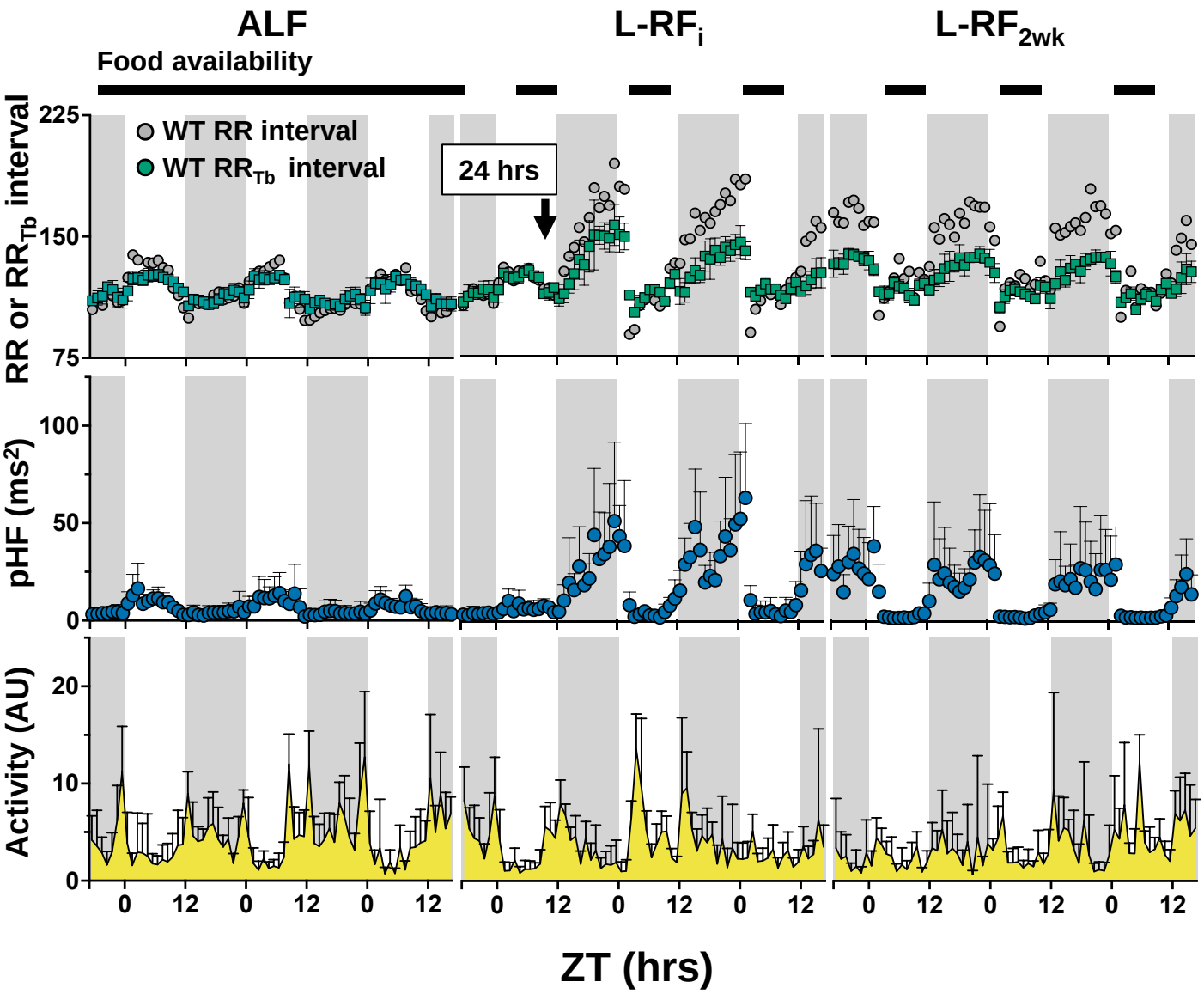
ALF
L-RF$_i$
L-RF$_{2wk}$
Food availability
WT RR interval
WT RR$_{Tb}$ interval
24 hrs
RR or RR$_{Tb}$ interval
225
150
75
pHF (ms^2)
100
50
0
Activity (AU)
20
10
0
0
12
ZT (hrs)

Figure 4.

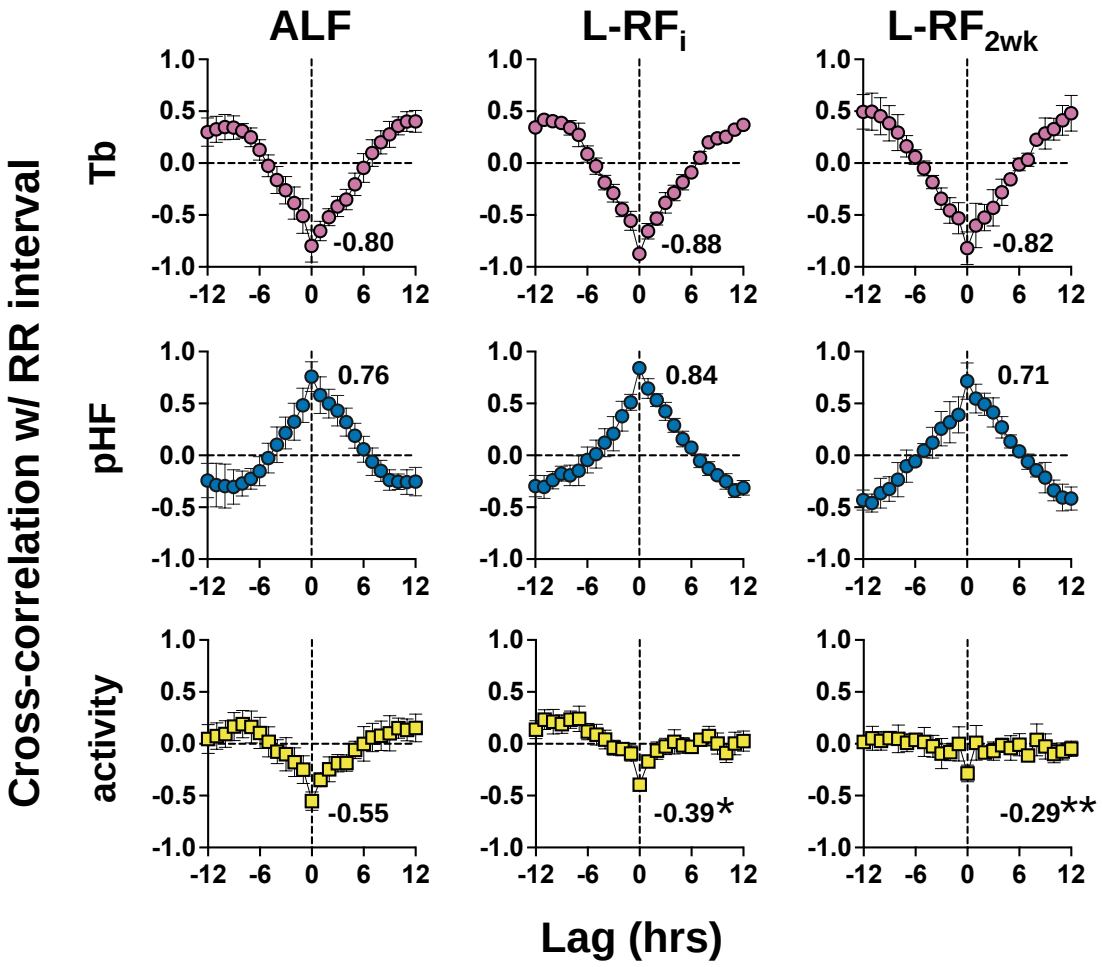
ALF
L-RF$_i$
L-RF$_{2wk}$
Tb
pHF
activity
Cross-correlation w/ RR interval
-0.80
-0.88
-0.82
0.76
0.84
0.71
-0.55
-0.39*
-0.29**
1.0
0.5
0.0
-0.5
-1.0
-12
-6
0
6
12
Lag (hrs)

Figure 5.

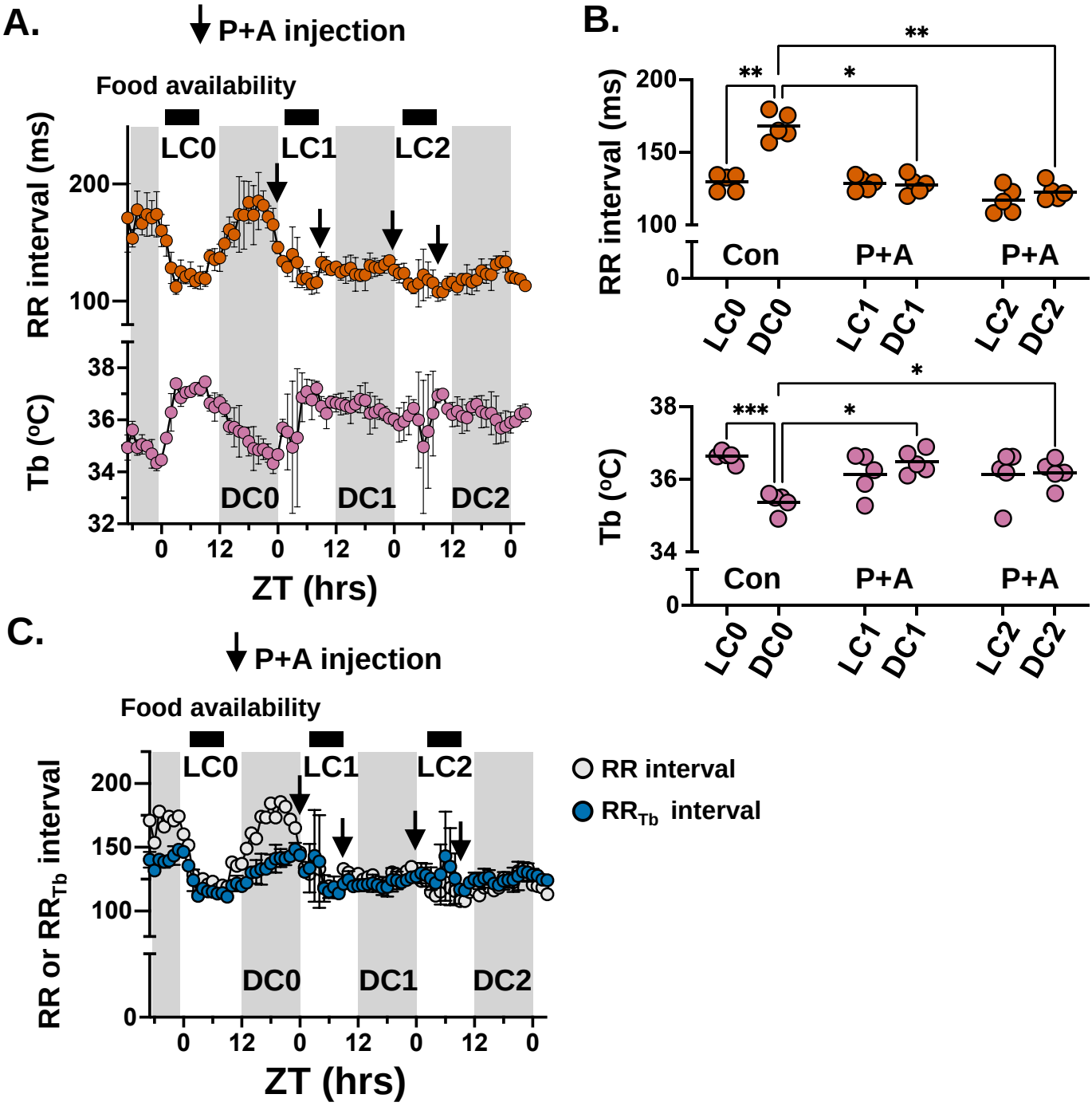
A.
P+A injection
Food availability
LC0
LC1
LC2
RR interval (ms)
200
100
Tb (ºC)
38
36
34
32
DC0
DC1
DC2
0
12
0
12
0
12
0
ZT (hrs)
B.
**
**
*
RR interval (ms)
200
150
100
0
Con
P+A
P+A
LC0
DC0
LC1
DC1
LC2
DC2
*
***
*
Tb (ºC)
38
36
34
0
Con
P+A
P+A
LC0
DC0
LC1
DC1
LC2
DC2
C.
P+A injection
Food availability
LC0
LC1
LC2
RR or RRTb interval
200
150
100
0
DC0
DC1
DC2
0
12
0
12
0
12
0
ZT (hrs)
RR interval
RRTb interval

Figure 6.

Thermoneutral

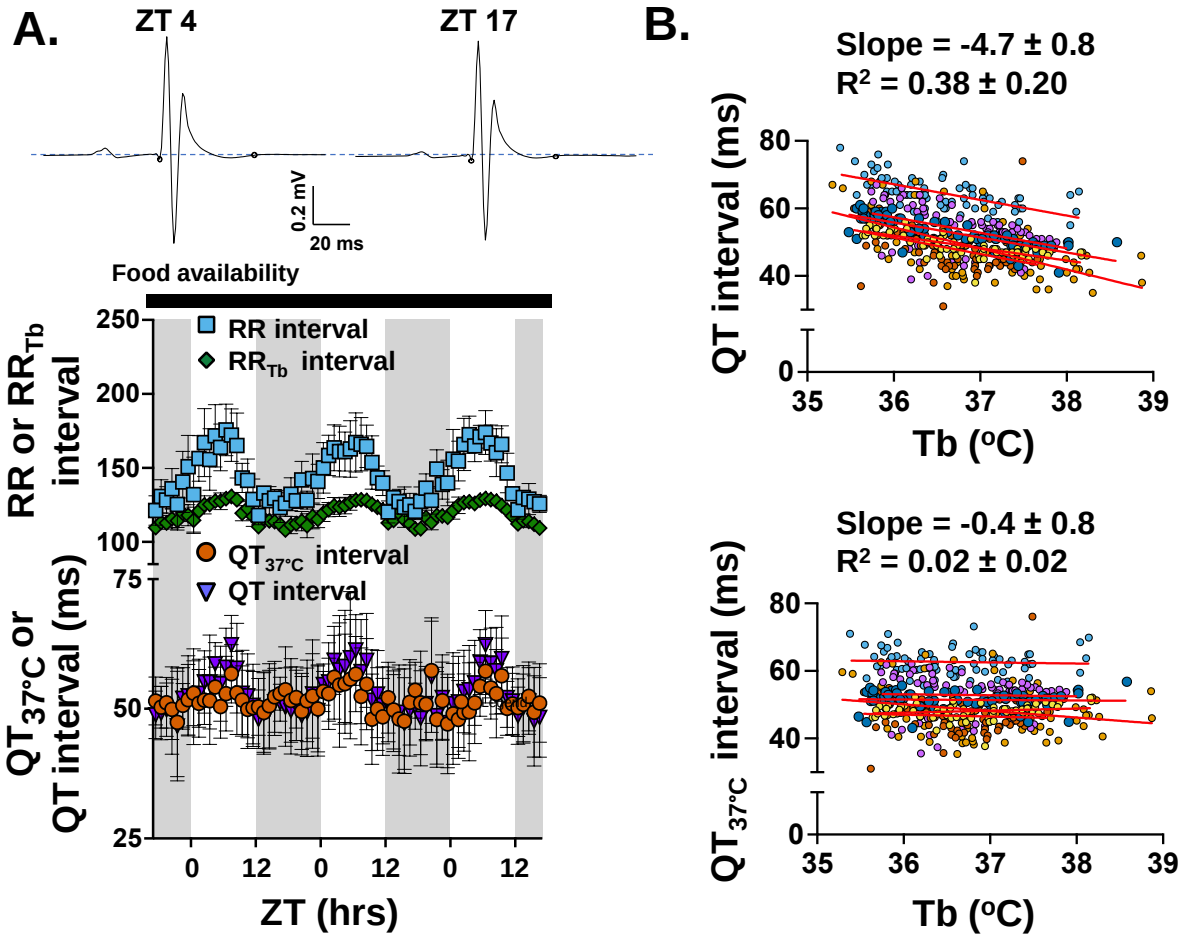

Figure 7.

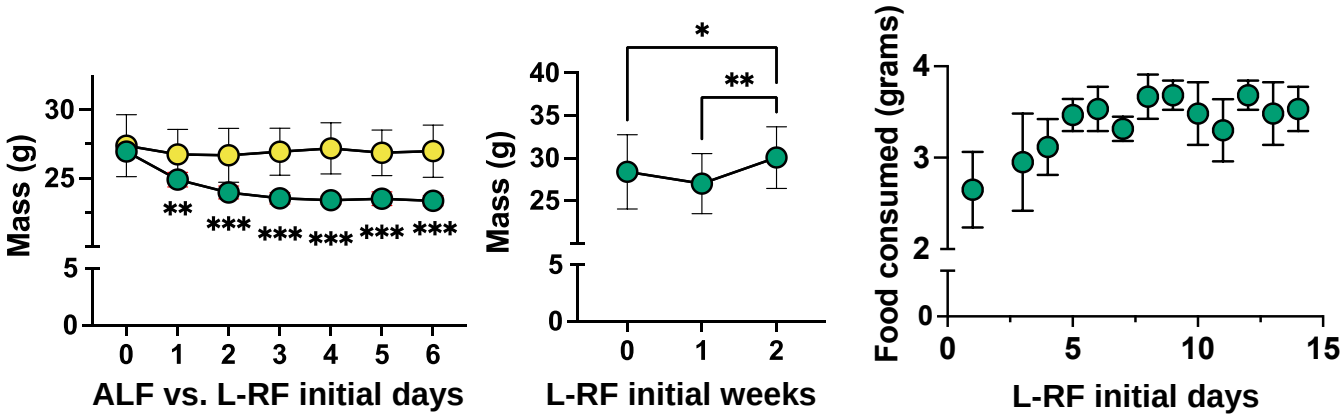

Supplement Figure 1.

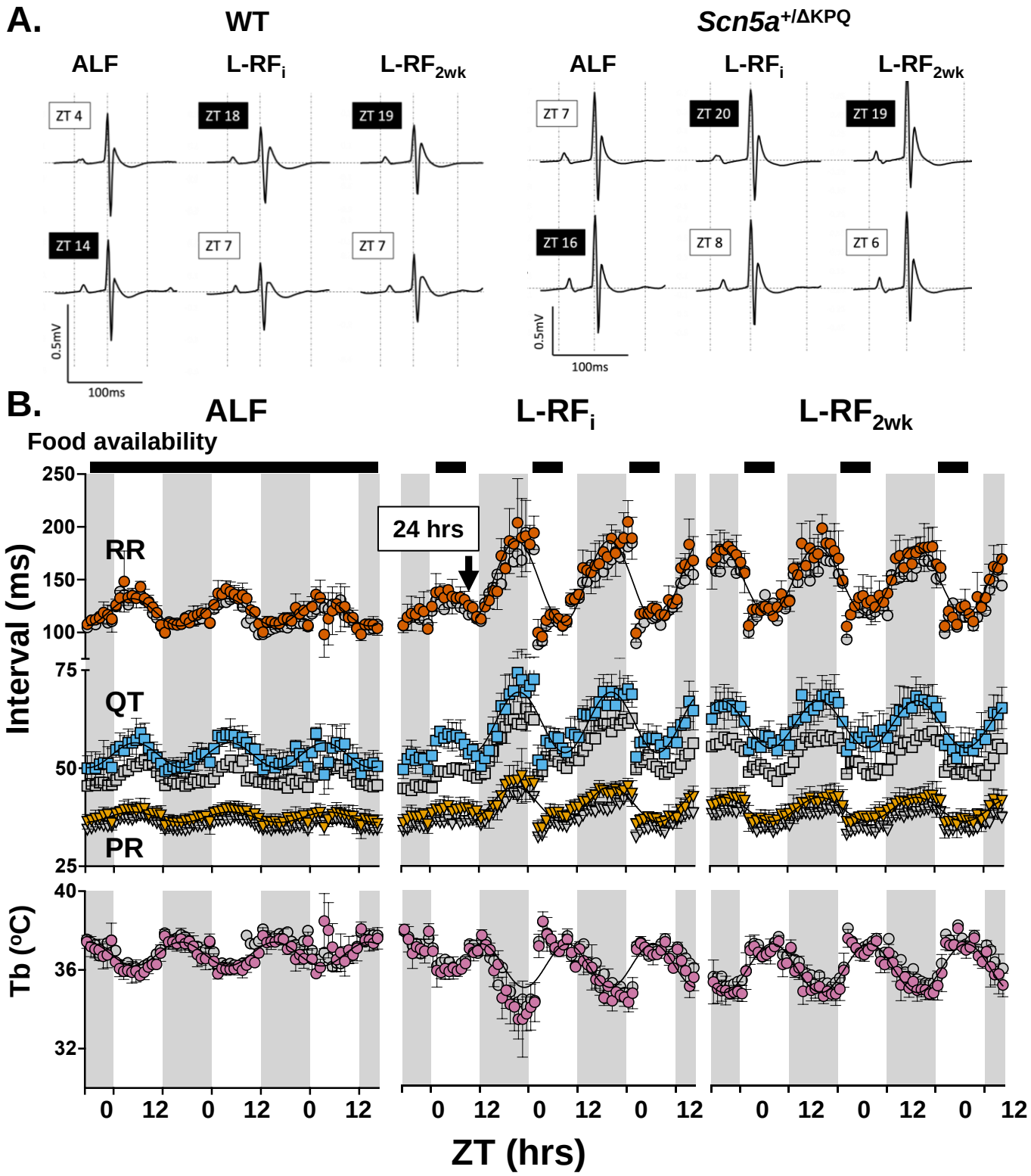

Supplement Figure 2.

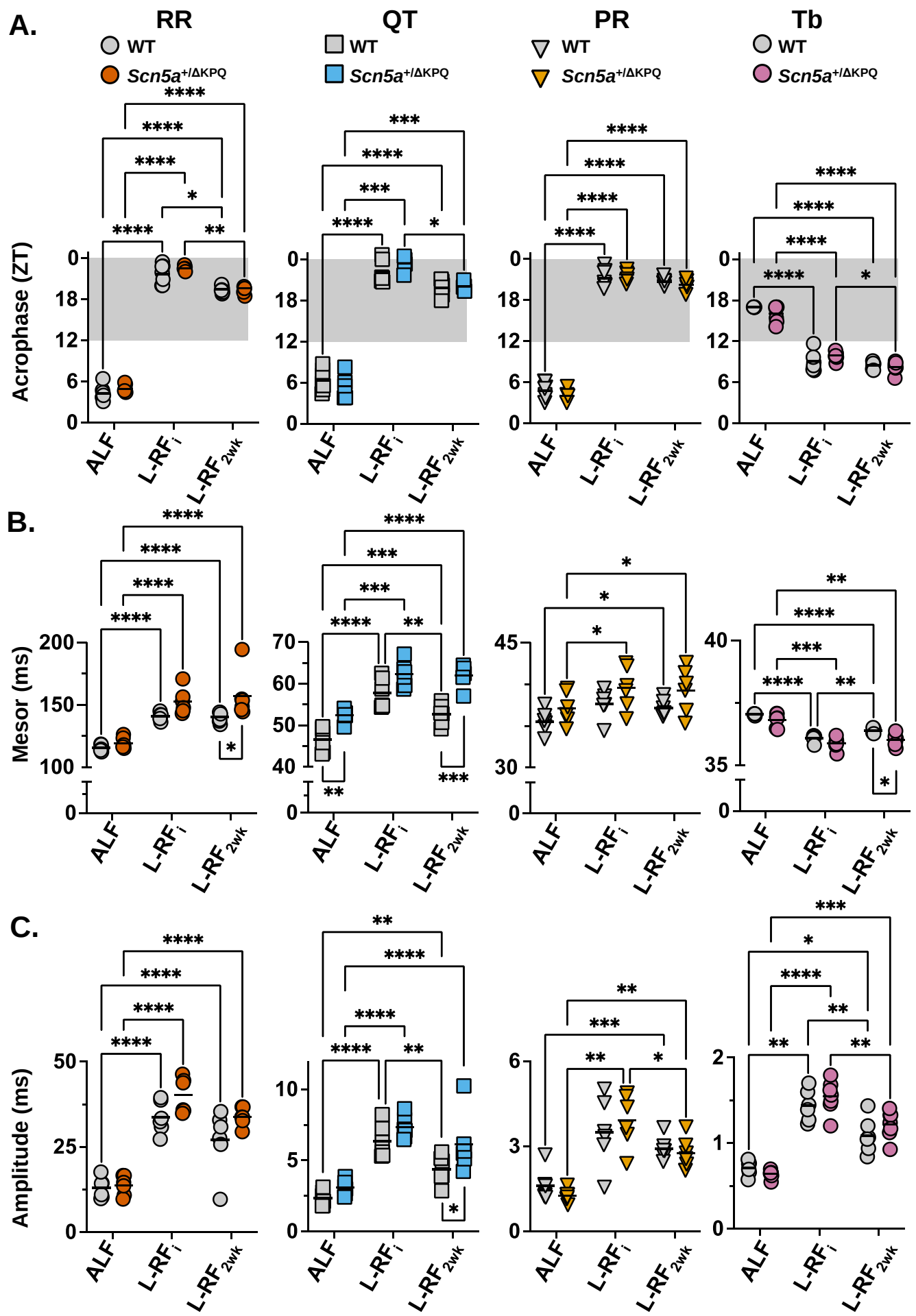

Supplement Figure 3.